

MambaDFuse: A Mamba-based Dual-phase Model for Multi-modality Image Fusion

Zhe Li
lizhe99@hrbeu.edu.cn
Harbin Engineering University

Haiwei Pan*
panhaiwei@hrbeu.edu.cn
Harbin Engineering University

Kejia Zhang
kejiazhang@hrbeu.edu.cn
Harbin Engineering University

Yuhua Wang
wangyuhua@hrbeu.edu.cn
Harbin Engineering University

Fengming Yu
yufengming@hrbeu.edu.cn
Harbin Engineering University

ABSTRACT

Multi-modality image fusion (MMIF) aims to integrate complementary information from different modalities into a single fused image to represent the imaging scene and facilitate downstream visual tasks comprehensively. In recent years, significant progress has been made in MMIF tasks due to advances in deep neural networks. However, existing methods cannot effectively and efficiently extract modality-specific and modality-fused features constrained by the inherent local reductive bias (CNN) or quadratic computational complexity (Transformers). To overcome this issue, we propose a Mamba-based Dual-phase Fusion (MambaDFuse) model. Firstly, a dual-level feature extractor is designed to capture long-range features from single-modality images by extracting low and high-level features from CNN and Mamba blocks. Then, a dual-phase feature fusion module is proposed to obtain fusion features that combine complementary information from different modalities. It uses the channel exchange method for shallow fusion and the enhanced Multi-modal Mamba (M3) blocks for deep fusion. Finally, the fused image reconstruction module utilizes the inverse transformation of the feature extraction to generate the fused result. Through extensive experiments, our approach achieves promising fusion results in infrared-visible image fusion and medical image fusion. Additionally, in a unified benchmark, MambaDFuse has also demonstrated improved performance in downstream tasks such as object detection. Code with checkpoints will be available after the peer-review process.

KEYWORDS

Image fusion, Mamba, multi-modality images, cross-modality interaction

1 INTRODUCTION

Image fusion aims to combine essential information representations from multiple source images to generate high-quality, content-enriched fused images [31, 49, 51, 52, 59]. Depending on the differences in imaging devices or imaging settings, image fusion can be categorized into various types, including multi-modality image fusion (MMIF) [22, 47, 58], digital photographic image fusion [31, 55], and remote sensing image fusion [2, 11, 50, 60]. Infrared-visible image fusion (IVF) and medical image fusion (MIF) are two typical tasks of MMIF, which model and fuse cross-modal features from all sensors. In particular, the infrared sensor captures thermal radiation

data, highlighting prominent targets, while the visible sensor captures reflected light information, producing digital images rich in texture details [27]. IVF aims to integrate complementary information from source images, resulting in high-contrast fusion images highlighting prominent targets while preserving rich texture details. These fusion images offer enhanced scene representation and visual perception, facilitating subsequent practical visual applications such as multi-modal saliency detection [19, 36, 43], object detection [3, 20, 42], and semantic segmentation [23, 33–35]. Similarly, in medical imaging, structural images such as computed tomography (CT) and magnetic resonance imaging (MRI) primarily provide structural and anatomical information [1], while functional images such as positron emission tomography (PET) and single-photon emission computed tomography (SPECT) reflect the metabolic activity of normal and pathological tissues and the cerebral blood flow signals [46]. MIF can precisely detect abnormal locations by integrating multiple imaging modalities, thereby assisting in diagnosis and treatment [10, 13].

In recent years, numerous methods have been developed to address challenges in MMIF. These methods primarily include Convolutional Neural Networks (CNNs) and AutoEncoders (AEs) [15, 17, 18, 58], Generative Adversarial Networks (GANs) [21, 28–30], Diffusion models [53, 57], as well as those based on Transformers [26, 37, 56]. The main drawback of the paradigms above is their inability to achieve both efficiency and effectiveness in MMIF. Firstly, CNN-based methods struggle to capture global context due to their limited receptive fields, making it challenging to generate high-quality fusion images. Moreover, using AE for feature extraction or image reconstruction poses challenges in designing an encoder that can capture modality-specific and shared features. Secondly, a pipeline based on generative models can generate high-quality fusion images but may not efficiently complete fusion tasks. GANs suffer from unstable training and mode collapse, while diffusion models face challenges such as long training time and slow sampling rate. Finally, models based on Transformers or a combination of Transformers and others exhibit excellent performance in global modeling but suffer from significant computational overhead due to the quadratic growth of resources with the number of token stemming from the self-attention mechanism.

The emergence of the improved S4, also known as Mamba [6], with its selective mechanism and efficient hardware-aware design, provides a novel solution to the challenges above. Mamba has been demonstrated to outperform Transformers in tasks requiring long-term dependency modeling, such as natural language processing,

*Corresponding authors.

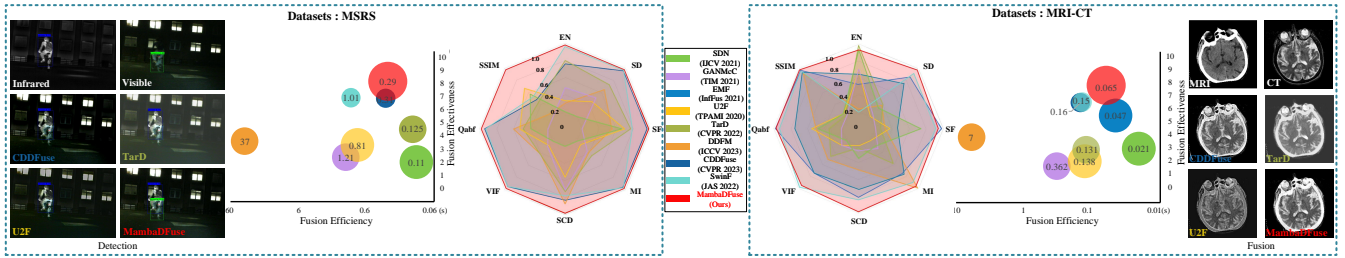


Figure 1: Fusion, detection and efficiency&effectiveness comparisons with state-of-the-art methods on MSRS and MRI-CT datasets. Octagons formed by lines of different colors represent the values of different methods across eight metrics. Our MambaDFuse outperforms the most comprehensive performance. The bubble chart illustrates the comparative analysis of efficiency and effectiveness, and the numbers inside the circles represent the time required to fuse a pair of images. Methods achieving similar fusion performance to ours demonstrate a slower fusion rate. Conversely, methods with a slightly faster rate than ours exhibit significantly lower fusion effectiveness. The fusion and detection results also showcase the powerful fusion capabilities of MambaDFuse. (The fusion metrics used in the chart are computed after normalization. The horizontal axis of the bubble chart represents time, while the vertical axis represents the sum of metrics.)

due to its input-adaptive and global information modeling capabilities while maintaining linear complexity, reducing computational costs, and enhancing inference speed. Recently, some variants of Mamba have also shown promising results in computer vision tasks, such as image classification [24, 61], medical image segmentation [25], and so on. However, Mamba’s role in the MMIF task has yet to be fully explored, as Mamba lacks a design similar to cross-attention. This prompts us to investigate how to utilize Mamba to integrate multi-modal information in MMIF.

Therefore, we propose a **Mamba**-based **Dual-phase Model for Multi-modality Image Fusion (MambaDFuse)**. It consists of three stages: a dual-level feature extraction, a dual-phase feature fusion, and fused image reconstruction. The hierarchical feature extraction consists of convolutional layers and multiple stacked Mamba blocks, leveraging the excellent processing capabilities of CNNs in the early stages of visual tasks and the efficiency of Mamba in extracting long-range features. Then, in feature fusion, the shallow fuse module utilizes manually designed fusion rules to fuse global overview features. In contrast, the deep fuse module conducts cross-modal deep feature fusion with improved Multi-modal Mamba (M3) blocks to obtain local detail features guided by the respective modality features. Ultimately, the fusion features are used to reconstruct the fused image. The loss function for reconstructing adopts the losses proposed in [26], consisting of SSIM loss, texture loss, and intensity loss, driving the network to preserve rich texture details and structural information while presenting optimal visual intensity. Fig. 1 demonstrates that our proposed MambaDFuse outperforms state-of-the-art methods in terms of subjective visual assessment and objective evaluation metrics.

Our main contributions can be summarized as follows:

- To the best of our knowledge, MambaDFuse is the first to leverage Mamba for MMIF, which is an alternative to CNNs and Transformers with effectiveness and efficiency.
- To capture low and high-level modality-specific features with long-range information, we design a dual-level feature extractor. The features encompass prominent objects, environmental lighting, and texture details.

- To get modality-fused features with global overview and local detail information, we propose a dual-phase feature fusion module. Specifically, channel exchange is used for shallow fuse, and an M3 block is designed for deep fuse.
- Our method achieves leading image fusion performance for both IVF and MIF. We also present a unified measurement benchmark to justify how the IVF fusion images facilitate downstream object detection.

2 RELATED WORKS

2.1 Multi-Modality image fusion

Multi-modality image fusion research based on deep learning leverages the powerful fitting capability of neural networks, enabling effective feature extraction and information fusion. According to the backbone of the models, existing methods can be classified into three categories: methods based on CNNs and AEs, methods employing generative models such as GANs and Diffusions, and methods utilizing Transformer (some in conjunction with CNN).

Firstly, for methods based on CNN and AE [15–17, 23, 54, 58], the typical pipeline involves feature extraction using CNNs or encoders, followed by image reconstruction using AEs. Utilizing context-agnostic CNNs is their limitation in extracting global information to generate high-quality fusion images, leading to a solid local reductive bias. Therefore, whether CNNs are sufficient for extracting features from all modalities remains to be seen. Additionally, careful consideration is required for encoder design. Shared encoders may fail to distinguish modality-specific features, while using separate encoders may overlook shared features between modalities.

Secondly, for methods based on generative models, GANs [21, 28–30] model the image fusion problem as an adversarial game between a generator and a discriminator, using adversarial training to generate fusion images with the same distribution as the source images. However, unstable training, lack of interpretability, and mode collapse have been critical issues affecting the generative capabilities of GANs. Also, diffusion models, consisting of diffusion and inverse diffusion stages, have achieved remarkable success

in image generation. However, when applied to the task of multi-modal image fusion [53, 57], an unresolved challenge is the high computational cost, resulting in long training and inference time, which impacts the efficiency of the fusion process.

Finally, methods based on Transformer or CNN-Transformer [26, 37, 56] have shown promising results due to their strong ability to model long-range dependencies. Transformers and their variants are used for feature extraction, fusion, and image reconstruction. However, the quadratic time complexity and computational resource consumption associated with the self-attention mechanism make them inefficient for multi-modal image fusion tasks. Even methods like [40], which use shifted window attention to improve performance, compromise long-term dependencies and fundamentally fail to address the quadratic complexity.

In conclusion, image fusion, a preprocessing step for advanced visual tasks, requires real-time processing and robust fusion capabilities. However, existing approaches have yet to achieve effective and efficient image fusion performance. Therefore, there is an urgent need for a new backbone to propel the progress and development of MMIF.

2.2 State Space Models (SSMs)

State Space Models (SSM) [7, 8, 40], originating from classical control theory [14], have become practical components for constructing deep networks due to their cutting-edge performance in analyzing continuous long sequential data. Structured State Space Sequence Models (S4) [7] represent pioneering work in state space models for modeling long-range dependencies. Subsequently, the S5 layer [40] was proposed based on S4, introducing a parallel scan on a diagonalized linear SSM. The H3 model [5] further refined and extended this work, enabling the model to achieve results comparable to Transformer in language modeling tasks.

A recent study named Mamba [6] further improved upon S4 by introducing a selection mechanism, enabling the model to choose relevant information depending on the input selectively. Simultaneously, a hardware-aware algorithm was proposed to achieve efficient training and inference. Compared to Transformer models of equivalent scale, Mamba exhibits higher inference speed, throughput, and overall performance. Subsequently, many works have extended Mamba from natural language processing (NLP) to other domains [12, 32, 44]. Visual Mamba (Vim) [61] applies Mamba to the Vision Transformer (ViT) architecture, proposing a novel universal visual backbone based on bidirectional Mamba blocks. This backbone embeds positional embeddings into image sequences and compresses visual representations through bidirectional state space models. Visual State Space Model (Vamba) [24] introduces a cross-scanning mechanism to bridge the gap between one-dimensional array scanning and two-dimensional plane traversal. In medical image segmentation tasks, Mamba has also been applied [25], yielding promising results. Since Mamba lacks a mechanism like cross-attention that facilitates the fusion of multi-modal information, research on effectively utilizing Mamba in MMIF is worthy of study.

In conclusion, similar to works such as [26], MambaDFuse comprises feature extraction, feature fusion, and image reconstruction.

However, what sets our approach apart is the utilization and enhancement of Mamba Blocks. Specifically, we design a dual-level feature extractor, an M3 block and a dual-phase feature fusion module tailored for MMIF. And through such a design, MambaDFuse can become a powerful tool in MMIF.

3 METHOD

3.1 Preliminaries

State space models (SSMs) are conventionally considered as a linear time-invariant system that builds a map stimulation from $x(t) \in \mathbb{R}^N$ to response $y(t) \in \mathbb{R}^N$ by a latent state $y(h) \in \mathbb{R}^N$. The system can be mathematically expressed using a linear ordinary differential equation (ODE):

$$h'(t) = Ah(t) + Bx(t) \quad (1)$$

$$y(t) = Ch(t) \quad (2)$$

where N is the state size, $A \in \mathbb{R}^{N \times N}$, $B \in \mathbb{R}^{N \times 1}$, and $C \in \mathbb{R}^{N \times 1}$.

As continuous-time models, SSMs pose significant challenges when incorporated into deep learning algorithms. To surmount this barrier, discretization becomes indispensable. We can discretize the system in Eq. 1 using the method of zero-order hold (ZOH), which can be formally defined as follows:

$$h_t = \bar{A}h_{t-1} + \bar{B}x_t \quad (3)$$

$$y_t = Ch_t \quad (4)$$

where $\bar{A} = \exp(\Delta A)$ and $\bar{B} = (\Delta A)^{-1}(\exp(\Delta A) - I) \cdot \Delta B$ are the discretized state parameters and Δ is the discretization step size.

However, the expression presented in Eq. 3 and 4 concentrates on the Linear Time-Invariant System with parameters that remain constant for different inputs. To overcome this constraint, Mamba [6] has sought to integrate a selective scanning mechanism, wherein the matrices B , C , and Δ are derived from the input data. In addition, by relying on a faster hardware-aware algorithm, Mamba has further advanced its potential.

3.2 Overall Architecture

The proposed MambaDFuse can be divided into three functional components: a dual-level feature extractor, a dual-phase feature fusion module, and a fused image reconstruction module. The detailed workflow is illustrated in Fig. 2. Assuming two different modalities of images, I_1 and I_2 , with I_f representing the fusion image, our pipeline can be described as follows:

Initially, dual-level feature extraction consists of low-level and high-level feature extraction. In the former, I_1 and I_2 are projected into a shared feature space by convolutional layers φ . However, the CNN layers may fail to capture global features due to their limited receptive fields. Therefore, after patch embedding, $N \times$ Mamba blocks ϕ are utilized for high-level feature extraction, yielding modality-specific features $F_n^{I_1}$ and $F_n^{I_2}$.

$$F_0^{I_1}, F_0^{I_2} = \text{PatchEmbed}(\varphi(I_1)), \text{PatchEmbed}(\varphi(I_2)) \quad (5)$$

$$F_n^{I_1} = \phi_{1n} \cdots \left(\phi_{11} \left(\phi_{10} \left(F_0^{I_1} \right) \right) \right) \quad (6)$$

$$F_n^{I_2} = \phi_{2n} \cdots \left(\phi_{21} \left(\phi_{20} \left(F_0^{I_2} \right) \right) \right) \quad (7)$$

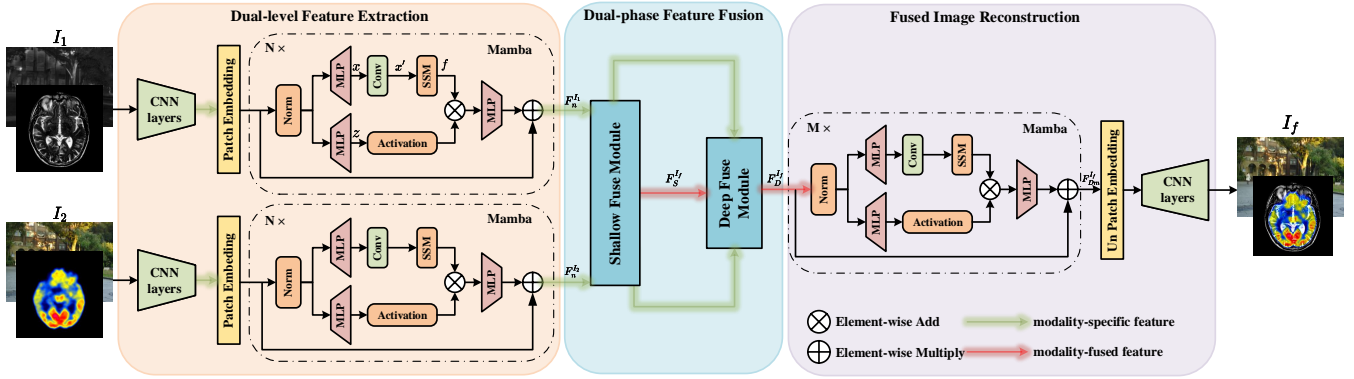


Figure 2: The overall architecture of MambaDFuse. It consists of three stages: dual-level feature extraction, dual-phase feature fusion, and fused image reconstruction.

Subsequently, in the shallow fuse module, a manually designed fusion strategy is employed to obtain an initial fusion feature $F_S^{I_f}$, including global integrated information. As for the local detail feature, we design an Multi-modal Mamba (M3) block to construct a deep fuse module, which utilizes multi-modal features as guidance to derive modality-fused feature $F_D^{I_f}$ for reconstruction.

$$F_n^{I_1}, F_n^{I_2}, F_S^{I_f} = \text{ShallowFuse} \left(F_n^{I_1}, F_n^{I_2} \right) \quad (8)$$

$$F_D^{I_f} = \text{DeepFuse} \left(F_n^{I_1}, F_n^{I_2}, F_S^{I_f} \right) \quad (9)$$

Lastly, in the fused image reconstruction stage, contrary to the feature extraction, the feature $F_D^{I_f}$ undergo $M \times$ Mamba blocks ϕ , followed by unpatchembedding, and finally, convolutional layers are applied to obtain the fused result I_f .

$$F_{Dm}^{I_f} = \phi_{fm} \cdots \left(\phi_{f1} \left(\phi_{f0} \left(F_{D0}^{I_f} \right) \right) \right) \quad (10)$$

$$I_f = \varphi \left(\text{UnPatchEmbed} \left(F_{Dm}^{I_f} \right) \right) \quad (11)$$

In the following sections (3.3 and 3.4), the detail and motivation of dual-level feature extraction and dual-phase feature fusion will be provided.

3.3 Dual-level Feature Extraction

Low-level Feature Extraction. Convolutional layers excel in early visual processing, enhancing optimization stability and superior outcomes [45]. Additionally, they provide a straightforward yet efficient means of capturing local semantic details and projecting them into a high-dimensional feature space. The Low-level Feature Extraction comprises two convolutional layers utilizing the Leaky ReLU activation function, each with a kernel size of 3×3 and a stride of 1.

High-level Feature Extraction. CNNs are constrained by local receptive fields when extracting features, while Transformers also encounter the issue of quadratic complexity. Considering this, mamba blocks are a promising choice for further extracting advanced modality-specific features. An input feature sequence $F_{t-1} \in \mathbb{R}^{B \times N \times C}$, firstly is applied layer normalization to obtain F'_{t-1} . Then, on two separate branches, F'_{t-1} is projected into x and z

Algorithm 1 High-level Feature Extraction.

Input: feature sequence $F_{t-1} : (B, N, C)$

Output: feature sequence $F_t : (B, N, C)$

- 1: $F'_{t-1} : (B, N, C) \leftarrow \text{LayerNorm}(F_{t-1})$
 - 2: $x : (B, N, C') \leftarrow \text{MLP}_x(F'_{t-1})$
 - 3: $z : (B, N, C') \leftarrow \text{MLP}_z(F'_{t-1})$
 - 4: $x' : (B, N, C') \leftarrow \text{SiLU}(\text{Conv}(x))$
/ Disc and SSM represents Eq. 3 and 4 implemented by selective scan [6] */*
 - 5: $\bar{A} : (B, N, C', D), \bar{B} : (B, N, C', D), C : (B, N, C', D) \leftarrow \text{Disc}(x')$
 - 6: $f : (B, N, C') \leftarrow \text{SSM}(\bar{A}, \bar{B}, C)(x')$
/ F_t represents modality-specific features */*
 - 7: $f' : (B, N, C') \leftarrow f \odot \text{SiLU}(z)$
 - 8: $F_t : (B, N, C) \leftarrow \text{MLP}_f(f') + F_{t-1}$
- return** F_t

using two multi-layer perceptrons (MLP). On the first branch, z undergoes convolution and SiLU activation to obtain x' . Subsequently, x' undergoes the State Space Model (Eq. 3 and 4) to compute f . On the other branch, z passes through a SiLU activation function to serve as a gating factor for gating f , resulting in f' . Finally, after an MLP layer and a residual connection, the output of the high-level feature extraction, F_t , is obtained. The detailed process is shown in Algorithm 1.

3.4 Dual-phase Feature Fusion

A practical fusion feature should incorporate significant information such as salient objects, environmental lighting, and texture details. A manually designed fusion rule can quickly produce an initial fusion feature in the first phase (as shown in Fig. 3 (a)). However, due to its inability to accommodate more complex fusion scenarios, an enhanced Mamba M3 block is utilized in the second phase (as shown in Fig. 4) to fuse deep texture detail features.

Shallow Fuse Module. Inspired by [4], we firstly adopt a channel exchange approach (Eq. 12) on $F_{t-1}^{I_1}$ and $F_{t-1}^{I_2}$, which does not require additional parameters or computational operations, to achieve lightweight exchange of features from multiple modalities. The exchanged features then undergo processing through their respective Mamba blocks. By repeating the above steps, modality-specific features $F_t^{I_1}$ and $F_t^{I_2}$ incorporate features from another modality, as

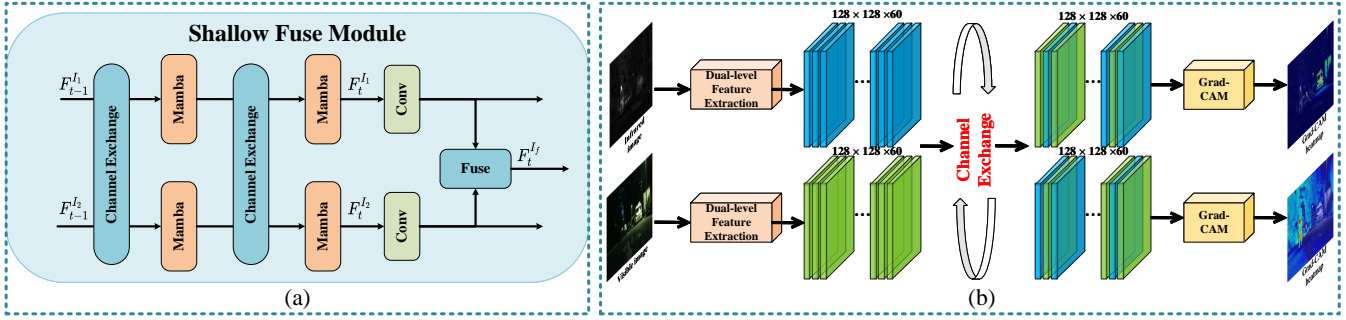


Figure 3: (a) is the implementation details of the shallow fuse module. (b) is channel exchange process and grad-cam [39] visualization results. The visualization is calculated for the output of Conv in the shallow fuse module. The heatmap demonstrates that the image has integrated information from the other modality after channel exchange, contributing to a shallow fuse.

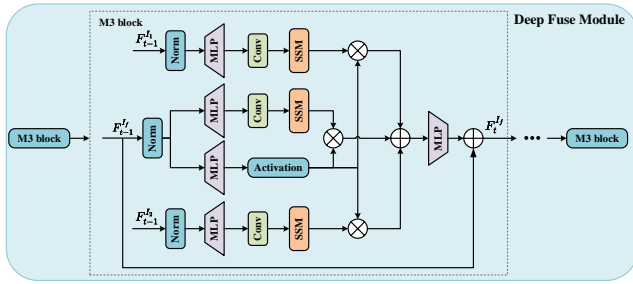


Figure 4: The implementation details of the deep fuse module.

illustrated in Fig. 3 (b). Subsequently, they undergo a FUSE operation to obtain a shallow fusion feature $F_t^{I_f}$. The FUSE operation can be addition or L1 normalization as proposed in [15].

$$F_{t-1}^{I_1/I_2} = \begin{cases} F_{t-1}^{I_1/I_2} & \text{if } M(B, N, C) = 0 \\ F_{t-1}^{I_2/I_1} & \text{if } M(B, N, C) = 1 \end{cases} \quad (12)$$

$M(B, N, C)$ refers to the mask used for channel exchange, consisting of 1s and 0s where 0 indicates no exchange and 1 indicates exchange.

Deep Fuse Module. The current Mamba architecture cannot directly handle multi-modal image information because it lacks mechanisms similar to cross-attention. As an improvement, we design a Multi-modal Mamba (M3) block. It utilizes modality-specific features to guide the generation of modality-fused features, aiming to incorporate local detail characteristics from different modalities inspired by [11]. The input is the initial fusion feature obtained from the shallow fuse module. Moreover, two additional branches are introduced, each taking features from different modalities as input. Similarly, these branches undergo layer normalization, convolution, SiLU activation, and parameter discretization and pass through the SSM to obtain an output y . After modulation by the gating factor, it is added to the output of the original branch, resulting in a final fusion feature. Please refer to the Algorithm 2 for specific details. A series of M3 blocks comprises the deep fuse module.

Algorithm 2 Multi-modal Mamba (M3) Block.

Input: feature sequence $F_{t-1}^{I_1} : (B, N, C)$, $F_{t-1}^{I_2} : (B, N, C)$, $F_{t-1}^{I_f} : (B, N, C)$
Output: feature sequence $F_t^{I_f} : (B, N, C)$

- 1: **for** o in $\{I_1, I_2, I_f\}$ **do**
- 2: $F_{t-1}^{o'} : (B, N, C) \leftarrow \text{LayerNorm}(F_{t-1}^o)$
- 3: $x_o : (B, N, C') \leftarrow \text{MLP}_{x_o}(F_{t-1}^{o'})$
- 4: $x'_o : (B, N, C') \leftarrow \text{SiLu}(\text{Conv}_o(x_o))$
- 5: $\bar{A} : (B, N, C', D)$, $\bar{B} : (B, N, C', D)$, $C : (B, N, C', D) \leftarrow \text{Disc}(x'_o)$
- 6: $y_o : (B, N, C') \leftarrow \text{SSM}(\bar{A}, \bar{B}, C)(x'_o)$
- 7: **end for**
- 8: $z : (B, N, C') \leftarrow \text{MLP}_z(F_{t-1}^{I_f})$
- 9: $y'_{I_1} : (B, N, C') \leftarrow y_{I_1} \odot \text{SiLu}(z)$
- 10: $y'_{I_2} : (B, N, C') \leftarrow y_{I_2} \odot \text{SiLu}(z)$
- 11: $F_t^{I_f} : (B, N, C) \leftarrow \text{MLP}_F(y'_{I_1} + y'_{I_2}) + F_{t-1}^{I_f}$
- return** $F_t^{I_f}$;

4 EXPERIMENTS

4.1 Setup

Datasets. For IVF experiments, three datasets are used to verify MambaDFuse, i.e., MSRS [41], RoadScene [48], and M³FD [21]. The training dataset consists of an MSRS training set (1083 pairs), 200 pairs in M³FD and 151 pairs in RoadScene, while an MSRS testing set (361 pairs), 100 pairs in M³FD and 70 pairs in RoadScene are employed as the testing dataset, which the fusion performance can be verified comprehensively. The datasets contain a diverse range of images captured night and day. Most images are taken on roads and include objects such as people, cars, bicycles, and road signs. For MIF experiments, we selected pairs of medical images from the Harvard Medical website [9], of which 48 pairs of MRI-CT images, 190 pairs of MRI-PET images, and 81 pairs of MRI-SPECT images.

Metrics. We use eight metrics to quantitatively measure the fusion results: entropy (EN), standard deviation (SD), mutual information (MI), sum of the correlations of differences (SCD), spatial frequency (SF), visual information fidelity (VIF), Qabf and structural similarity index measure (SSIM). Higher metrics imply that a fusion image is better.

Table 1: Quantitative results of the IVF task. Red and blue show the best and second-best values, respectively.

Datasets: MSRS Fusion Dataset								
	EN	SD	SF	MI	SCD	VIF	Qabf	SSIM
SDN	5.40	19.14	9.14	1.75	1.10	0.55	0.39	0.38
GANMcC	5.85	28.54	6.18	2.38	1.46	0.60	0.30	0.30
U2F	5.61	26.80	9.39	1.98	1.36	0.59	0.45	0.40
TarD	6.35	35.49	9.89	2.65	1.48	0.67	0.43	0.35
DDFM	5.56	32.84	8.43	2.47	1.58	0.67	0.48	0.31
CDDFuse	6.29	42.47	11.18	4.67	1.55	0.98	0.64	0.36
SwinF	6.61	43.69	10.02	4.71	1.51	0.97	0.63	0.37
Ours	6.67	43.74	11.35	4.78	1.67	1.00	0.66	0.47
Datasets: RoadScene Fusion Dataset								
	EN	SD	SF	MI	SCD	VIF	Qabf	SSIM
SDN	7.35	50.02	15.35	3.47	1.65	0.61	0.50	0.45
GANMcC	7.13	48.41	10.64	2.90	1.72	0.51	0.39	0.41
U2F	7.22	42.23	14.94	2.84	1.59	0.57	0.51	0.28
TarD	7.23	45.69	12.17	3.44	1.39	0.55	0.43	0.43
DDFM	7.36	49.07	13.36	3.05	1.65	0.60	0.50	0.47
CDDFuse	7.43	52.31	14.62	3.14	1.71	0.62	0.45	0.45
SwinF	6.92	46.68	12.80	3.35	1.61	0.59	0.44	0.46
Ours	7.38	51.30	15.68	3.62	1.62	0.66	0.56	0.49
Datasets: M ³ FD Fusion Dataset								
	EN	SD	SF	MI	SCD	VIF	Qabf	SSIM
SDN	6.67	40.83	14.85	3.37	1.65	0.60	0.52	0.46
GANMcC	6.65	39.02	10.75	2.88	1.72	0.56	0.37	0.41
U2F	6.67	38.48	14.70	2.75	1.82	0.68	0.56	0.47
TarD	6.68	40.02	12.87	3.17	1.51	0.59	0.42	0.44
DDFM	6.52	35.56	11.08	2.88	1.81	0.66	0.54	0.45
CDDFuse	6.66	39.96	17.26	3.85	1.68	0.82	0.59	0.48
SwinF	6.72	37.52	14.22	4.10	1.60	0.73	0.60	0.47
Ours	6.81	40.19	16.89	4.26	1.75	0.76	0.61	0.48

Implement details. The experiments use two NVIDIA GeForce RTX 4090 GPUs. A batch size 12 is employed, and each fusion task undergoes 10,000 training steps. During each step, images from the training set are randomly cropped into patches of size 128×128 , which are subsequently normalized to fall within the range $[0, 1]$. The parameters of MambaDFuse are optimized using the Adam optimizer, with the learning rate set to 2×10^{-5} . The loss function is similar to that used in SwinFusion.

For RGB inputs. We adopt the same processing approach as previous work. Firstly, the RGB images are converted to the YCbCr color space, where the Y channel represents the luminance channel, and the Cb and Cr channels represent chrominance. Only the Y channel is utilized for fusion. Subsequently, the fused Y, Cb, and Cr channels are converted back to the RGB color space through inverse mapping.

4.2 Comparison with SOTA methods

In this section, MambaDFuse is compared with the state-of-the-art methods, including the CNN and AE-based methods group: SDN [54], EMF [46], U2F [47]; and the generative methods group: GANMcC [30], TarD [21], DDFM [57]; and the Transformer-based methods group: CDDFuse [56], SwinF [26]. Among them, EMF is

Table 2: Quantitative results of the MIF task. Red and blue show the best and second-best values, respectively.

Datasets: MRI-CT Medical Fusion Dataset								
	EN	SD	SF	MI	SCD	VIF	Qabf	SSIM
SDN	4.80	59.26	28.17	2.39	0.98	0.35	0.39	0.19
GANMcC	4.55	54.58	16.57	2.43	0.88	0.38	0.28	0.16
EMF	4.49	79.58	22.20	2.81	1.36	0.56	0.50	0.64
U2F	4.54	52.48	20.33	2.31	0.82	0.38	0.42	0.19
TarD	4.87	62.41	17.86	2.65	0.85	0.45	0.34	0.17
DDFM	4.06	61.57	19.00	3.03	1.12	0.47	0.40	0.62
CDDFuse	4.37	84.01	33.81	2.80	1.45	0.56	0.60	0.66
SwinF	4.03	87.14	31.93	2.94	1.59	0.66	0.57	0.65
Ours	4.80	90.95	32.43	2.99	1.65	0.64	0.60	0.67
Datasets: MRI-PET Medical Fusion Dataset								
	EN	SD	SF	MI	SCD	VIF	Qabf	SSIM
SDN	2.42	63.82	30.44	2.47	1.38	0.47	0.58	0.55
GANMcC	4.98	58.64	16.29	2.23	0.92	0.29	0.24	0.45
EMF	4.73	60.91	25.69	2.79	1.57	0.58	0.58	0.52
U2F	4.61	60.46	22.54	1.15	1.21	0.40	0.49	0.47
TarD	5.01	56.73	19.88	2.80	0.83	0.53	0.44	0.51
DDFM	4.39	63.79	18.95	3.64	1.25	0.44	0.45	0.49
CDDFuse	4.94	67.84	27.26	3.23	1.25	0.64	0.59	0.50
SwinF	3.90	71.13	30.33	2.93	1.50	0.63	0.68	0.51
Ours	4.91	73.05	30.45	3.08	1.59	0.65	0.68	0.52
Datasets: MRI-SPECT Medical Fusion Dataset								
	EN	SD	SF	MI	SCD	VIF	Qabf	SSIM
SDN	3.80	44.74	20.24	2.40	1.27	0.58	0.64	0.62
GANMcC	4.16	44.61	11.41	1.86	1.10	0.31	0.21	0.36
EMF	3.98	42.86	15.09	2.40	0.88	0.66	0.67	0.59
U2F	3.98	50.01	15.74	1.97	1.09	0.39	0.47	0.58
TarD	4.25	48.43	15.32	2.32	1.01	0.56	0.53	0.36
DDFM	3.89	43.57	12.92	2.99	1.05	0.49	0.44	0.56
CDDFuse	4.09	52.12	18.10	3.19	1.19	0.82	0.60	0.61
SwinF	3.90	54.18	20.10	3.03	1.54	0.81	0.72	0.63
Ours	3.99	55.43	20.50	3.32	1.63	0.81	0.75	0.64

an architecture designed specifically for the MIF task, so it is not compared in the IVF task.

Quantitative comparison. Eight metrics are employed to quantitatively compare the above results, which are displayed in Tab. 1 and 2. MambaDFuse exhibited remarkable performance across nearly all metrics, confirming its applicability to various lighting conditions and object categories. In the results of our method, higher values of MI, Qabf, and SSIM indicate a higher amount of information transferred from the source images to the fused image with minimal distortion. Better SD suggests that MambaDFuse demonstrates improved contrast. Meanwhile, the excellent performance of SF also implies richer edge and texture details. The improved VIF further confirms that its ability aligns with human visual perception.

Qualitative comparison. Subsequently, we show the qualitative comparison in Fig. 5, 6 and 7. MambaDFuse effectively integrates thermal radiation information from infrared images with detailed texture and illumination information from visible images. Consequently, objects located in dimly-lit environments are conspicuously accentuated, enabling easy distinguishing of foreground objects

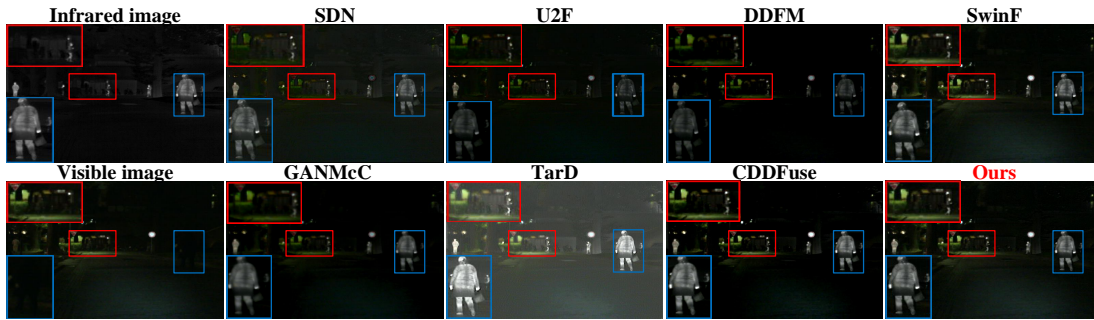


Figure 5: Visual comparison for “00718N” in MSRS IVF dataset.

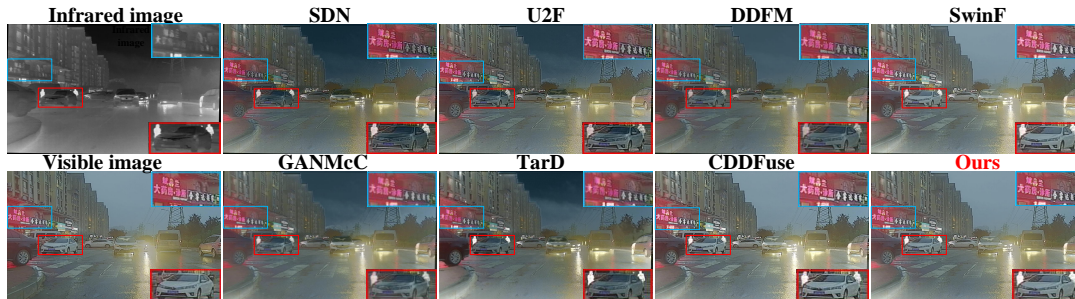


Figure 6: Visual comparison for “00033” in M³FD IVF dataset.

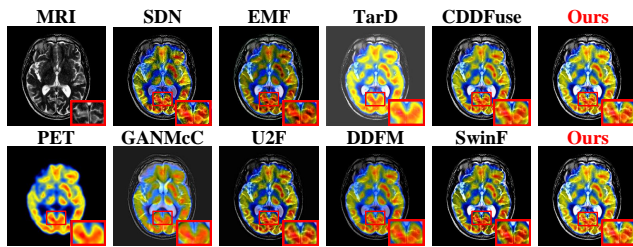


Figure 7: Visual comparison for MRI-PET MIF dataset.

from the background. Moreover, previously indistinct background features due to low illumination now possess clearly defined edges and abundant contour information, enhancing their ability to comprehend the scene.

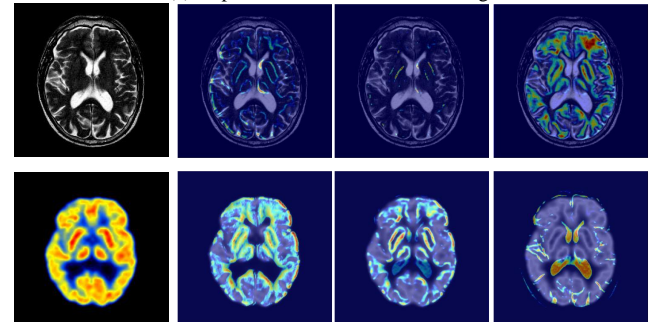
4.3 Ablation Study

Ablation experiments are conducted to verify the rationality of the different designs and modules. EN, SD, VIF, MI, VIF, and Qabf are utilized to validate the fusion effectiveness quantitatively. The results of the experimental groups are presented in Tab. 3.

We performed ablation experiments across three stages: feature extraction, feature fusion, and fused image reconstruction. In the feature extraction stage, the effectiveness of high-level feature extraction was verified. In the feature fusion stage, experiments were performed by removing the shallow and deep fuse modules separately. The results showed a decrease in performance in both cases,



(a) : a pair of infrared and visible images



(b) : a pair of MRI and PET images

Figure 8: Grad-CAM visualization results. Similar to Fig. 3 (b), we performed feature visualization on different options in the shallow fuse module and found that the features obtained using channel exchange excelled at integrating information from the other modality.

Table 3: Ablation experiment results in the test set of MSRS. Red indicates the best value.

	EN	SD	SF	MI	VIF	Qabf
Feature Extraction						
I.w/o high-level feature extraction	6.65	43.7	11.24	4.47	0.97	0.64
Shallow Fuse Module						
II.w/o shallow fuse module	6.66	43.7	11.29	4.65	0.98	0.65
III.no swap & no exchange	6.66	43.7	11.3	4.67	0.99	0.65
IV.channel exchange → channel swap	6.66	43.69	11.34	4.75	1.00	0.65
Deep Fuse Module						
V.w/o deep fuse module	6.66	43.72	11.27	4.59	0.98	0.64
VI.one modal as guidance	6.65	43.68	11.21	4.5	0.97	0.64
VII.another modal as guidance	6.65	43.67	11.24	4.57	0.98	0.64
Reconstruction						
VIII.w/o Mamba blocks	6.65	43.68	11.26	4.47	0.97	0.64
Ours	6.67	43.74	11.35	4.78	1.00	0.66

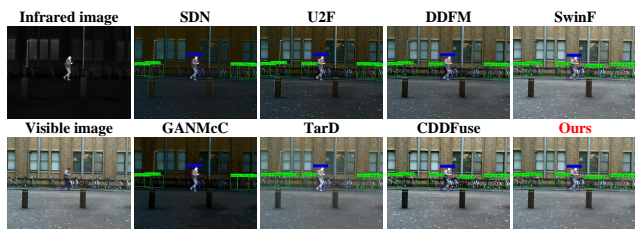


Figure 9: Results of object detection. The fused images obtained from MambaDFuse preserve both thermal radiation information and illumination information. Therefore, it makes objects in the image clearer and more distinguishable, achieving the best detection results.

demonstrating the necessity of both phases of feature fusion. Additionally, in the shallow fuse module, we investigated the options of using channel swap [11], channel exchange for feature interchange, or neither. Fig. 8 visualizes the features, confirming the effectiveness of channel exchange in the module. In the deep fuse module, we ablated the selection of guiding in M3 block and found that the optimal metrics were achieved only when both modalities were used for guidance. Finally, in the fused image reconstruction, ablation experiments are conducted by removing the Mamba Blocks, confirming the design’s rationale.

Table 4: The object detection performance (mAP) of visible, infrared, and fused images obtained from different methods on the MSRS dataset. Red and blue show the best and second-best values, respectively.

	AP@0.5			AP@0.7			AP@0.9		
	Person	Car	All	Person	Car	All	Person	Car	All
Infrared	0.940	0.593	0.767	0.932	0.579	0.756	0.884	0.533	0.709
Visible	0.683	0.917	0.800	0.669	0.914	0.792	0.614	0.880	0.747
SDN	0.949	0.908	0.929	0.939	0.911	0.92	0.863	0.904	0.863
GANMcC	0.895	0.954	0.919	0.889	0.870	0.909	0.789	0.825	0.852
U2F	0.951	0.919	0.931	0.936	0.913	0.926	0.854	0.876	0.876
TarD	0.929	0.927	0.928	0.927	0.923	0.921	0.859	0.888	0.873
DDFM	0.928	0.936	0.932	0.917	0.931	0.924	0.837	0.890	0.863
CDDFuse	0.933	0.883	0.908	0.929	0.88	0.905	0.867	0.831	0.849
SwinF	0.896	0.945	0.92	0.883	0.891	0.912	0.873	0.863	0.868
Ours	0.950	0.940	0.935	0.937	0.921	0.925	0.889	0.893	0.879

4.4 Downstream IVF applications

The purpose of MMIF is to facilitate further visual task applications, such as object detection, semantic segmentation, etc. Therefore, to determine the effectiveness of a method, the fused images should be utilized in downstream tasks to assess whether they positively contribute to these tasks. In our work, IVF image fusion is adopted for object detection. Eighty pairs of infrared and visible images were selected from the MSRS dataset, mainly annotated with people and cars. All fused images, together with the original infrared and visible images, were subjected to object detection using a pre-trained YOLOv5 model [38] (trained on the COCO dataset). Tab. 4 presents the mean average precision (mAP), where AP@0.5, AP@0.7, and AP@0.9 denote the AP values at IoU thresholds of 0.5, 0.7, and 0.9, respectively. It was observed that visible images and infrared images provide limited information individually. For instance, object detectors are more likely to detect cars in visible images and people in infrared images. However, our fused images complement each other, providing a more comprehensive description of the scene and making it easier to detect both people and cars without any shortcomings. Among the various fusion methods compared, MambaDFuse demonstrates the best detection performance. Fig. 9 also provides a visualized example.

5 CONCLUSION

In this paper, we explore Mamba’s potential for multi-modality image fusion for the first time, proposing an efficient and effective Mamba-based dual-phase model and designing an Multi-modal Mamba (M3) block. On the one hand, dual-level feature extraction improves the extraction of modality-specific features. On the other hand, the dual-phase feature fusion module facilitates synthesizing comprehensive and complementary modality-fused features. Extensive experiments demonstrate that MambaDFuse can achieve promising fusion results and improve the accuracy of downstream tasks such as object detection.

REFERENCES

- [1] Mohamed Awad, Ahmed Elliethy, and Hussein A Aly. 2019. Adaptive near-infrared and visible fusion for fast image enhancement. *IEEE Transactions on Computational Imaging* 6 (2019), 408–418.
- [2] Wele Gedara Chaminda Bandara and Vishal M Patel. 2022. HyperTransformer: A textural and spectral feature fusion transformer for pansharpening. In *Proceedings of the IEEE/CVF conference on computer vision and pattern recognition*. 1767–1777.
- [3] Alexey Bochkovskiy, Chien-Yao Wang, and Hong-Yuan Mark Liao. 2020. Yolov4: Optimal speed and accuracy of object detection. *arXiv preprint arXiv:2004.10934* (2020).
- [4] Sheng Fang, Kaiyu Li, and Zhe Li. 2023. Changer: Feature interaction is what you need for change detection. *IEEE Transactions on Geoscience and Remote Sensing* (2023).
- [5] Daniel Y Fu, Tri Dao, Khaled K Saab, Armin W Thomas, Atri Rudra, and Christopher Ré. 2022. Hungry hungry hippos: Towards language modeling with state space models. *arXiv preprint arXiv:2212.14052* (2022).
- [6] Albert Gu and Tri Dao. 2023. Mamba: Linear-time sequence modeling with selective state spaces. *arXiv preprint arXiv:2312.00752* (2023).
- [7] Albert Gu, Karan Goel, and Christopher Ré. 2021. Efficiently modeling long sequences with structured state spaces. *arXiv preprint arXiv:2111.00396* (2021).
- [8] Albert Gu, Isys Johnson, Karan Goel, Khaled Saab, Tri Dao, Atri Rudra, and Christopher Ré. 2021. Combining recurrent, convolutional, and continuous-time models with linear state space layers. *Advances in neural information processing systems* 34 (2021), 572–585.
- [9] Harvard medical website. [n. d.]. *Harvard medical website*. <http://www.med.harvard.edu/AANLIB/home.html>.
- [10] Chunming He, Kai Li, Guoxia Xu, Jiangpeng Yan, Longxiang Tang, Yulun Zhang, Yaowei Wang, and Xiu Li. 2023. Hqg-net: Unpaired medical image enhancement with high-quality guidance. *IEEE Transactions on Neural Networks and Learning Systems* (2023).
- [11] Xuanhua He, Ke Cao, Keyu Yan, Rui Li, Chengjun Xie, Jie Zhang, and Man Zhou. 2024. Pan-Mamba: Effective pan-sharpening with State Space Model. *arXiv preprint arXiv:2402.12192* (2024).
- [12] Md Mohaiminul Islam, Mahmudul Hasan, Kishan Shamsundar Athrey, Tony Braskich, and Gedas Bertasius. 2023. Efficient movie scene detection using state-space transformers. In *Proceedings of the IEEE/CVF Conference on Computer Vision and Pattern Recognition*. 18749–18758.
- [13] Alex Pappachen James and Belur V Dasarathy. 2014. Medical image fusion: A survey of the state of the art. *Information fusion* 19 (2014), 4–19.
- [14] Rudolph Emil Kalman. 1960. A new approach to linear filtering and prediction problems. (1960).
- [15] Hui Li and Xiao-Jun Wu. 2018. DenseFuse: A fusion approach to infrared and visible images. *IEEE Transactions on Image Processing* 28, 5 (2018), 2614–2623.
- [16] Hui Li, Xiao-Jun Wu, and Tariq Durrani. 2020. NestFuse: An infrared and visible image fusion architecture based on nest connection and spatial/channel attention models. *IEEE Transactions on Instrumentation and Measurement* 69, 12 (2020), 9645–9656.
- [17] Hui Li, Xiao-Jun Wu, and Josef Kittler. 2021. RFN-Nest: An end-to-end residual fusion network for infrared and visible images. *Information Fusion* 73 (2021), 72–86.
- [18] Pengwei Liang, Junjun Jiang, Xianming Liu, and Jiayi Ma. 2022. Fusion from decomposition: A self-supervised decomposition approach for image fusion. In *European Conference on Computer Vision*. Springer, 719–735.
- [19] Aishan Liu, Xianglong Liu, Jiaxin Fan, Yuqing Ma, Anlan Zhang, Huiyuan Xie, and Dacheng Tao. 2019. Perceptual-sensitive gan for generating adversarial patches. In *Proceedings of the AAAI conference on artificial intelligence*, Vol. 33. 1028–1035.
- [20] Aishan Liu, Xianglong Liu, Hang Yu, Chongzhi Zhang, Qiang Liu, and Dacheng Tao. 2021. Training robust deep neural networks via adversarial noise propagation. *IEEE Transactions on Image Processing* 30 (2021), 5769–5781.
- [21] Jinyuan Liu, Xin Fan, Zhanbo Huang, Guanyao Wu, Risheng Liu, Wei Zhong, and Zhongxuan Luo. 2022. Target-aware dual adversarial learning and a multi-scenario multi-modality benchmark to fuse infrared and visible for object detection. In *Proceedings of the IEEE/CVF conference on computer vision and pattern recognition*. 5802–5811.
- [22] Jinyuan Liu, Xin Fan, Ji Jiang, Risheng Liu, and Zhongxuan Luo. 2021. Learning a deep multi-scale feature ensemble and an edge-attention guidance for image fusion. *IEEE Transactions on Circuits and Systems for Video Technology* 32, 1 (2021), 105–119.
- [23] Risheng Liu, Zhu Liu, Jinyuan Liu, and Xin Fan. 2021. Searching a hierarchically aggregated fusion architecture for fast multi-modality image fusion. In *Proceedings of the 29th ACM International Conference on Multimedia*. 1600–1608.
- [24] Yue Liu, Yunjie Tian, Yuzhong Zhao, Hongtian Yu, Lingxi Xie, Yaowei Wang, Qixiang Ye, and Yunfan Liu. 2024. Vmamba: Visual state space model. *arXiv preprint arXiv:2401.10166* (2024).
- [25] Jun Ma, Feifei Li, and Bo Wang. 2024. U-mamba: Enhancing long-range dependency for biomedical image segmentation. *arXiv preprint arXiv:2401.04722* (2024).
- [26] Jiayi Ma, Linfeng Tang, Fan Fan, Jun Huang, Xiaoguang Mei, and Yong Ma. 2022. SwinFusion: Cross-domain long-range learning for general image fusion via swin transformer. *IEEE/CAA Journal of Automatica Sinica* 9, 7 (2022), 1200–1217.
- [27] Jiayi Ma, Linfeng Tang, Meilong Xu, Hao Zhang, and Guobao Xiao. 2021. STD-FusionNet: An infrared and visible image fusion network based on salient target detection. *IEEE Transactions on Instrumentation and Measurement* 70 (2021), 1–13.
- [28] Jiayi Ma, Han Xu, Junjun Jiang, Xiaoguang Mei, and Xiao-Ping Zhang. 2020. DDcGAN: A dual-discriminator conditional generative adversarial network for multi-resolution image fusion. *IEEE Transactions on Image Processing* 29 (2020), 4980–4995.
- [29] Jiayi Ma, Wei Yu, Pengwei Liang, Chang Li, and Junjun Jiang. 2019. FusionGAN: A generative adversarial network for infrared and visible image fusion. *Information fusion* 48 (2019), 11–26.
- [30] Jiayi Ma, Hao Zhang, Zhenfeng Shao, Pengwei Liang, and Han Xu. 2020. GAN-McC: A generative adversarial network with multiclassification constraints for infrared and visible image fusion. *IEEE Transactions on Instrumentation and Measurement* 70 (2020), 1–14.
- [31] Kede Ma, Zhengfang Duanmu, Hojatollah Yeganeh, and Zhou Wang. 2017. Multi-exposure image fusion by optimizing a structural similarity index. *IEEE Transactions on Computational Imaging* 4, 1 (2017), 60–72.
- [32] Eric Nguyen, Karan Goel, Albert Gu, Gordon Downs, Preey Shah, Tri Dao, Stephen Baccus, and Christopher Ré. 2022. S4nd: Modeling images and videos as multidimensional signals with state spaces. *Advances in neural information processing systems* 35 (2022), 2846–2861.
- [33] Haotong Qin, Yifu Ding, Mingyuan Zhang, Qinghua Yan, Aishan Liu, Qingqing Dang, Ziwei Liu, and Xianglong Liu. 2022. Bibert: Accurate fully binarized bert. *arXiv preprint arXiv:2203.06390* (2022).
- [34] Haotong Qin, Ruihao Gong, Xianglong Liu, Mingzhu Shen, Ziran Wei, Fengwei Yu, and Jingkuan Song. 2020. Forward and backward information retention for accurate binary neural networks. In *Proceedings of the IEEE/CVF conference on computer vision and pattern recognition*. 2250–2259.
- [35] Haotong Qin, Xiangguo Zhang, Ruihao Gong, Yifu Ding, Yi Xu, and Xianglong Liu. 2023. Distribution-sensitive information retention for accurate binary neural network. *International Journal of Computer Vision* 131, 1 (2023), 26–47.
- [36] Xuebin Qin, Zichen Zhang, Chenyang Huang, Chao Gao, Masood Dehghan, and Martin Jagersand. 2019. Basnet: Boundary-aware salient object detection. In *Proceedings of the IEEE/CVF conference on computer vision and pattern recognition*. 7479–7489.
- [37] Linhao Qu, Shaolei Liu, Manning Wang, and Zhijian Song. 2022. Transmf: A transformer-based multi-exposure image fusion framework using self-supervised multi-task learning. In *Proceedings of the AAAI conference on artificial intelligence*, Vol. 36. 2126–2134.
- [38] Joseph Redmon, Santosh Divvala, Ross Girshick, and Ali Farhadi. 2016. You only look once: Unified, real-time object detection. In *Proceedings of the IEEE conference on computer vision and pattern recognition*. 779–788.
- [39] Ramprasaath R Selvaraju, Michael Cogswell, Abhishek Das, Ramakrishna Vedantam, Devi Parikh, and Dhruv Batra. 2017. Grad-cam: Visual explanations from deep networks via gradient-based localization. In *Proceedings of the IEEE international conference on computer vision*. 618–626.
- [40] Jimmy TH Smith, Andrew Warrington, and Scott W Linderman. 2022. Simplified state space layers for sequence modeling. *arXiv preprint arXiv:2208.04933* (2022).
- [41] Linfeng Tang, Jiteng Yuan, Hao Zhang, Xingyu Jiang, and Jiayi Ma. 2022. PI-Fusion: A progressive infrared and visible image fusion network based on illumination aware. *Information Fusion* 83 (2022), 79–92.
- [42] Shiyu Tang, Ruihao Gong, Yan Wang, Aishan Liu, Jiakai Wang, Xinyun Chen, Fengwei Yu, Xianglong Liu, Dawn Song, Alan Yuille, et al. 2021. Robuststart: Benchmarking robustness on architecture design and training techniques. *arXiv preprint arXiv:2109.05211* (2021).
- [43] Jiakai Wang, Aishan Liu, Zixin Yin, Shunchang Liu, Shiyu Tang, and Xianglong Liu. 2021. Dual attention suppression attack: Generate adversarial camouflage in physical world. In *Proceedings of the IEEE/CVF Conference on Computer Vision and Pattern Recognition*. 8565–8574.
- [44] Jue Wang, Wentao Zhu, Pichao Wang, Xiang Yu, Linda Liu, Mohamed Omar, and Raffay Hamid. 2023. Selective structured state-spaces for long-form video understanding. In *Proceedings of the IEEE/CVF Conference on Computer Vision and Pattern Recognition*. 6387–6397.
- [45] Tete Xiao, Mannat Singh, Eric Mintun, Trevor Darrell, Piotr Dollár, and Ross Girshick. 2021. Early convolutions help transformers see better. *Advances in neural information processing systems* 34 (2021), 30392–30400.
- [46] Han Xu and Jiayi Ma. 2021. EMFusion: An unsupervised enhanced medical image fusion network. *Information Fusion* 76 (2021), 177–186.
- [47] Han Xu, Jiayi Ma, Junjun Jiang, Xiaojie Guo, and Haibin Ling. 2020. U2Fusion: A unified unsupervised image fusion network. *IEEE Transactions on Pattern Analysis and Machine Intelligence* 44, 1 (2020), 502–518.
- [48] Han Xu, Jiayi Ma, Zhuliang Le, Junjun Jiang, and Xiaojie Guo. 2020. FusionDn: A unified densely connected network for image fusion. In *Proceedings of the AAAI conference on artificial intelligence*, Vol. 34. 12484–12491.

- [49] Ruikang Xu, Zeyu Xiao, Mingde Yao, Yueyi Zhang, and Zhiwei Xiong. 2021. Stereo video super-resolution via exploiting view-temporal correlations. In *Proceedings of the 29th ACM International Conference on Multimedia*. 460–468.
- [50] Shuang Xu, Jiangshe Zhang, Zixiang Zhao, Kai Sun, Junmin Liu, and Chunxia Zhang. 2021. Deep gradient projection networks for pan-sharpening. In *Proceedings of the IEEE/CVF Conference on Computer Vision and Pattern Recognition*. 1366–1375.
- [51] Zizheng Yang, Mingde Yao, Jie Huang, Man Zhou, and Feng Zhao. 2022. Sir-former: Stereo image restoration using transformer. In *Proceedings of the 30th ACM International Conference on Multimedia*. 6377–6385.
- [52] Mingde Yao, Zhiwei Xiong, Lizhi Wang, Dong Liu, and Xuejin Chen. 2019. Spectral-depth imaging with deep learning based reconstruction. *Optics express* 27, 26 (2019), 38312–38325.
- [53] Jun Yue, Leyuan Fang, Shaobo Xia, Yue Deng, and Jiayi Ma. 2023. Dif-fusion: Towards high color fidelity in infrared and visible image fusion with diffusion models. *IEEE Transactions on Image Processing* (2023).
- [54] Hao Zhang and Jiayi Ma. 2021. SDNet: A versatile squeeze-and-decomposition network for real-time image fusion. *International Journal of Computer Vision* 129, 10 (2021), 2761–2785.
- [55] Xingchen Zhang. 2021. Deep learning-based multi-focus image fusion: A survey and a comparative study. *IEEE Transactions on Pattern Analysis and Machine Intelligence* 44, 9 (2021), 4819–4838.
- [56] Zixiang Zhao, Haowen Bai, Jiangshe Zhang, Yulun Zhang, Shuang Xu, Zudi Lin, Radu Timofte, and Luc Van Gool. 2023. Cddfuse: Correlation-driven dual-branch feature decomposition for multi-modality image fusion. In *Proceedings of the IEEE/CVF conference on computer vision and pattern recognition*. 5906–5916.
- [57] Zixiang Zhao, Haowen Bai, Yuanzhi Zhu, Jiangshe Zhang, Shuang Xu, Yulun Zhang, Kai Zhang, Deyu Meng, Radu Timofte, and Luc Van Gool. 2023. DDFM: denoising diffusion model for multi-modality image fusion. In *Proceedings of the IEEE/CVF International Conference on Computer Vision*. 8082–8093.
- [58] Zixiang Zhao, Shuang Xu, Chunxia Zhang, Junmin Liu, Pengfei Li, and Jiangshe Zhang. 2020. DIDFuse: Deep image decomposition for infrared and visible image fusion. *arXiv preprint arXiv:2003.09210* (2020).
- [59] Zixiang Zhao, Shuang Xu, Chunxia Zhang, Junmin Liu, and Jiangshe Zhang. 2020. Bayesian fusion for infrared and visible images. *Signal Processing* 177 (2020), 107734.
- [60] Zixiang Zhao, Jiangshe Zhan, Shuang Xu, Kai Sun, Lu Huang, Junmin Liu, and Chunxia Zhang. 2021. FGF-GAN: A lightweight generative adversarial network for pansharpening via fast guided filter. In *2021 IEEE International Conference on Multimedia and Expo (ICME)*. IEEE, 1–6.
- [61] Lianghui Zhu, Bencheng Liao, Qian Zhang, Xinlong Wang, Wenyu Liu, and Xinggang Wang. 2024. Vision mamba: Efficient visual representation learning with bidirectional state space model. *arXiv preprint arXiv:2401.09417* (2024).